Available online at www.sciencedirect.com
ScienceDirect
Magnetic Resonance Imaging xx (2008) xxx – xxx
MAGNETIC RESONANCE IMAGING

Quantification of venous blood signal contribution to BOLD functional activation in the auditory cortex at 3 T

Sergio Casciaro[a,b,*], Roberto Bianco[b], Alessandro Distante[a,b]

[a]Biomedical Engineering Division, National Council of Research, Institute of Clinical Physiology, 73100 Lecce, Italy
[b]Bioengineering Division, Euro Mediterranean Scientific Biomedical Institute, 72100 Brindisi, Italy

Received 19 October 2007; revised 23 February 2008; accepted 24 February 2008

Abstract

Most modern techniques for functional magnetic resonance imaging (fMRI) rely on blood-oxygen-level-dependent (BOLD) contrast as the basic principle for detecting neuronal activation. However, the measured BOLD effect depends on a transfer function related to neurophysiological changes accompanying electrical neural activation. The spatial accuracy and extension of the region of interest are determined by vascular effect, which introduces incertitude on real neuronal activation maps. Our efforts have been directed towards the development of a new methodology that is capable of combining morphological, vascular and functional information; obtaining new insight regarding foci of activation; and distinguishing the nature of activation on a pixel-by-pixel basis. Six healthy volunteers were studied in a parametric auditory functional experiment at 3 T; activation maps were overlaid on a high-resolution brain venography obtained through a novel technique. The BOLD signal intensities of vascular and nonvascular activated voxels were analyzed and compared: it was shown that nonvascular active voxels have lower values for signal peak ($P<10^{-7}$) and area ($P<10^{-8}$) with respect to vascular voxels. The analysis showed how venous blood influenced the measured BOLD signals, supplying a technique to filter possible venous artifacts that potentially can lead to misinterpretation of fMRI results. This methodology, although validated in the auditory cortex activation, maintains a general applicability to any cortical fMRI study, as the basic concepts on which it relies on are not limited to this cortical region. The results obtained in this study can represent the basis for new methodologies and tools that are capable of adding further characterization to the BOLD signal properties.

Keywords: Functional magnetic resonance imaging (fMRI); Quantification of venous blood signals; BOLD contrast; Auditory cortex; Brain venography; Venous artifacts

1. Introduction

Since the discovery of the blood-oxygen-level-dependent (BOLD) effect in the early 1990s [1,2], MRI has gained great importance in the study of brain function and morphology [3]. The preliminary work by Ogawa et al. was followed by a series of studies that have tried to provide physiological explanations to the BOLD effect theory [4,5], as well as a quantitative modeling of the phenomenon [6,7]. It is known that neuronal activity induces in the local microvasculature transient variations in regional hemodynamics in terms of cerebral blood flow, cerebral blood volume and blood oxygenation [8,9]. In particular, activation causes a temporary rise in the oxygenation level, with consequent decrease in blood deoxyhemoglobin (dHb) content. Since dHb acts as a paramagnetic intrinsic contrast agent, the final result is a typical increase in the MR signal [10].

However, one of the main issues related to BOLD functional magnetic resonance imaging (fMRI) is that the spatial relation between cortical activation sites and the location of task-related hemodynamic changes is uncertain [11]. As a consequence, BOLD activation maps may be corrupted by venous artifacts, and concern about the actual meaning of fMRI images arises [12]. These issues suggest

* Corresponding author. National Research Council, Institute of Clinical Physiology, Biomedical Engineering Division, c/o Campus Univesitario Ecotekne, via per Monteroni, 73100 Lecce, Italy. Tel.: +39 0832 422 310; fax: +39 0832 422 341.
E-mail address: casciaro@ifc.cnr.it (S. Casciaro).

0730-725X/$ – see front matter © 2008 Elsevier Inc. All rights reserved.
doi:10.1016/j.mri.2008.02.006

caution when using the results of BOLD fMRI, especially for specific applications such as neurosurgery [13] where high confidence and high reliability in the maps provided by functional studies are required.

So far, several attempts have been made to investigate the relationship between BOLD activation and vascular structures. All of these studies faced the problem by merging information obtained from anatomical and functional MR scans and by trying to characterize the signal coming from vascular regions.

In a study conducted by Hlustik et al. [14], several subjects were scanned at 1.5 T during a motor task (finger tapping). Magnetic resonance angiograms were acquired as 2D phase-contrast angiograms (PCAs), and these were used to remove venous-activated regions. The highest resolution of PCA, though, is limited by the minimum detectable flow determined by scanner sensitivity [15]. Moreover, pulse sequence and velocity encoding have to be chosen to maximize scanner sensitivity to blood flow measures within a specific range of vessel diameters [16]. Finally, to account for the different resolutions of the angiograms and functional images, the former was smoothed with a Gaussian filter, with further loss of in-plane resolution.

In Krings et al. [17], the process of venous-activated voxel detection was performed using, as anatomical references, a PCA and a set of contrast-enhanced T_1-weighted images, which were acquired after the injection of gadolinium diethyltriaminepentaacetic acid. The results of this study show that venous voxels have a higher percentage of signal change and a longer signal rise time. This study has the same limitations associated with using PCA, as discussed above, while the improved information provided by the contrast-enhanced images is obtained at the expense of the increased invasiveness of the exam.

Hall et al. [18] used a 3-T scanner and performed tissue classification into four categories through a gray-level thresholding procedure on different kinds of MR images. Venography was performed with time-of-flight (TOF) venous-weighted images, with the venous weighting determined in accordance with the phase-masking method described by Reichenbach et al. [19]. However, the logistic regression proposed in their work depends on parameters obtained by γ-curve fitting and not on actual MR signal. Thus, this approach lacks general validity. This limitation is of particular concern in light of the fact that the BOLD signal curve changes with the basic aspects of experimental design (e.g., block- or event-related designs) [20] Thus, different analytical functions have been used to fit BOLD time series, such as boxcar functions [21], sinusoids [22] or others obtained from the linear model theory [23].

We propose a method that exploits the enhanced performance of a modern 3-T scanner with optimal pulse sequence parameters to obtain high-resolution (<0.5 mm, in-plane) brain venography. Combining morphological and vascular information with the functional datasets on a pixel-by-pixel basis, we managed to quantify with high accuracy the venous content of each activated voxel and to characterize the signal. A correlation study between signal and stimulus duration uncovered different response patterns when comparing venous and nonvenous voxels. These results support the use of this method in characterizing venous-activated voxels with high precision, without the need for invasive procedures or contrast agent injections.

2. Methods

2.1. Subjects and task

Six healthy volunteers (aged 23–65 years) were provided with acoustic stimulation during an fMRI experiment; all subjects gave prior written consent. The acoustic stimulation was programmed with the commercial software *Presentation* (Neurobehavioral Systems, Inc., Albany, CA) and delivered to the subjects by means of headphones.

The stimulation pattern consisted of a 1000-Hz tone with 2-s duration, followed by a rest period lasting 18 s, for an overall time of 20 s. This pattern was repeated 20 times consecutively, and the results of all runs were averaged to increase the signal-to-noise ratio (SNR). The beginning of the stimulation was preceded by a 20-s period of rest as baseline. The total time of the functional scan was 420 s.

The repetition time of the stimuli was set to 20 s in order to avoid the response overlapping of two consecutive stimuli and to allow for an event-related experiment [24].

2.2. MR scans

The subjects were imaged with a GE 3-T Signa (General Electric, Fairfield, CT) clinical scanner using head coils.

Two sets of high-resolution anatomical images were acquired for each subject, namely, T_1-weighted and T_2*-weighted images. Both datasets were made up of 40 images covering the same volume and corresponding to the regions of the auditory cortex.

The T_1-weighted images were obtained with a 3D spoiled gradient recalled echo (SPGR) sequence with the following imaging parameters: T_R=18 ms, T_E=3 ms, flip angle=15°, field of view=24×24 cm^2, image matrix=512×512, voxel size=0.47×0.47×1 mm^3, scan time=3 min 26 s.

The T_2*-weighted images were also acquired with a 3D SPGR sequence. Imaging parameters were as follows: T_R=30 ms, T_E=25 ms, flip angle=25°, field of view=24×24 cm^2, image matrix=512×512, voxel size=0.47×0.47×1 mm^3, scan time=7 min 34 s.

For the functional scan, a gradient-echo (GE) echo planar imaging (EPI) sequence was used throughout the stimulation, which gave sets of 10 T_2*-weighted axial slices [25]. The imaging parameters were as follows: T_R=1 s, T_E=30 ms, flip angle=90°, field of view=20×20 cm^2, image matrix=64×64, voxel size=3.7×3.7×3 mm^3. Four hundred

twenty volumes were acquired for each subject, with a sampling time of 1 s.

2.3. Image processing

The images were assembled with AFNI software [26] into two anatomical datasets (T_1 weighted and T_2* weighted) and a functional dataset.

The functional dataset was first registered with a rigid-body algorithm available in AFNI to correct movements of the subjects during the functional study. The registered dataset was then averaged, obtaining a dataset made up of 20 volumes sampled every 1 s.

The T_2* anatomical dataset and the functional dataset were resampled at a common scale (2 mm) in order to obtain two datasets with the same number of voxels. The T_2* anatomical dataset was then registered to the functional datasets. The rigid transformation was applied to the original high-resolution T_2* anatomical dataset to avoid the interpolation or filtering of the functional dataset.

The T_1-weighted anatomical dataset was registered to the T_2*-weighted anatomical dataset.

Scalp stripping was performed on both anatomical datasets by means of a brain segmentation procedure.

The T_1- and T_2*-weighted anatomical datasets were filtered with an anisotropic diffusion filter [27] in order to increase the SNR of the images and to make the following segmentation procedure more reliable.

A fuzzy C-means clustering procedure [28,29] was applied to the T_1 and T_2* anatomical datasets, setting the number of clusters to three. The three clusters correspond to the three tissues making up the brain: white matter, gray matter and cerebrospinal fluid (CSF). Indeed, as veins produce low MR signals because of local spin dephasing [30], in the T_2* dataset, the cluster with the lowest intensity level includes also veins along with the CSF (see the Discussion section). The fuzzy segmentation was transformed into a hard segmentation by assigning each voxel to the tissue with the highest membership function. Venous vessels were then segmented by subtracting from the voxels of the CSF+veins class in the T_2* dataset those belonging to the CSF class of the T_1 dataset.

2.4. Data analysis

In the functional datasets, activated areas were found through cross-correlation of the voxel time course with a model function $r(t)$, obtained through convolution of the stimulus and the γ-variate hemodynamic function as used by Cohen [23]. A correlation threshold of $r=.75$ was used as the statistical threshold ($P<2.2\times10^{-4}$, uncorrected). The time series of the activated voxels were expressed as percent change from the baseline, with the latter calculated as the mean of the signal in the rest period preceding the start of the stimulation.

Merging the high-resolution venous map with the activation map, it was possible to assess whether each active voxel was associated with a macroscopic vein. Active voxels were thus classified either as “venous” or as “nonvenous”; “venous” voxels are those found in correspondence with macroscopic veins detected by the segmentation procedure, while “nonvenous” voxels are those for which no macroscopic vein was detected. The peaks and the areas under the signal of these two classes were compared through a t test.

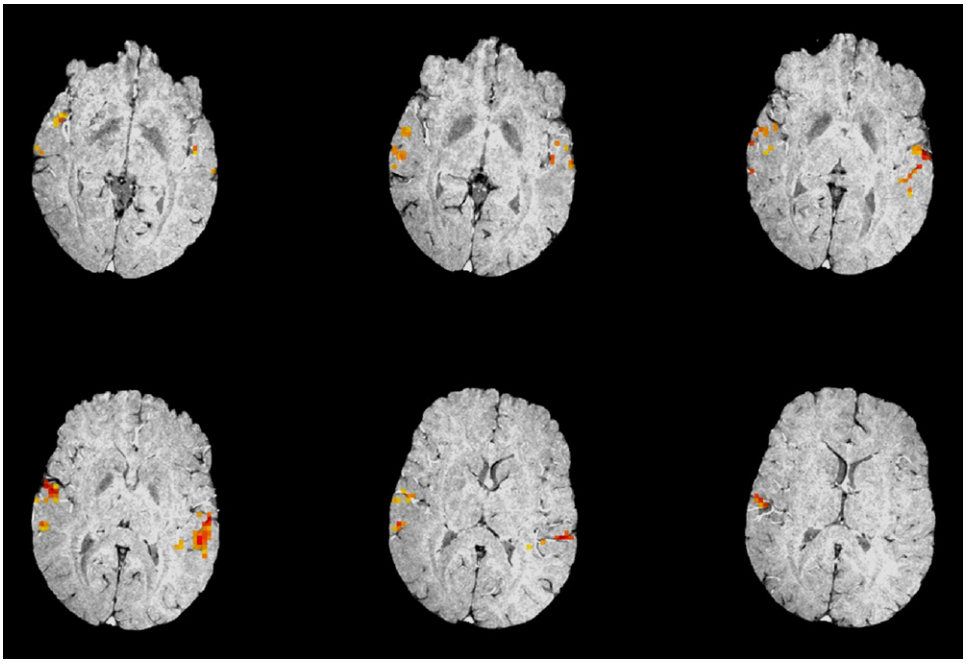

Fig. 1. Activated areas in S4 ($r>.75$).

The area under the signal was estimated as the sum of all the signal values sampled at 1 s and expressed in arbitrary units.

3. Results

The analysis of MR images revealed functional activation of the auditory cortex in all subjects. Fig. 1 shows representative regions of activation developing bilaterally in the auditory cortex of S4. Activation was strongly clustered into two or three distinct areas partly corresponding to Heschl's gyri, indicated by location, length and inclination, as recognizable from a visual comparison with anatomical atlases of the brain. These results are typical of those observed in other experiments utilizing auditory stimuli [31].

Table 1 summarizes the major results of all subjects. A variable quantity of activated voxels was found across subject datasets, with a mean value of 71 (±43.6 S.D.). The mean percent signal peak in all subjects was in the range 1.2–2.9%. Fig. 2 shows the average time course for the "venous" and "nonvenous" active voxels for all subjects (Fig. 2, left-hand side, S1–S6). Of note, in the mean time course of three subjects (S3, S4 and S6), a poststimulus undershoot is evident. The plot on the right-hand side ('Average') of Fig. 2 illustrates instead the average of the mean time series of all subjects.

Venous and nonvenous voxels were found in different proportions across the subjects. The percentage of nonvenous voxels in each subject ranged from 18% to 56% (Table 1).

Fig. 3 shows, as an example, the brain venous vasculature underlying regions of activation for one brain section. The vasculature is depicted as a projection of the venogram obtained from the vein segmentation performed as described in the Methods section.

Finally, Figs. 4 and 5 represent the histogram of the values of the peaks and areas under the curve for the populations of vascular and nonvascular voxels across all subjects. It can be appreciated how both, in the case of the peaks and the areas, the nonvascular voxels tend to show lower values with a small spread, while the vascular voxels present a higher mean value with a wider dispersion. The average values of the peaks of the nonvenous and venous populations are, respectively, 1.4% and 2.3%, while for the areas, the values are 5.5% and 9.3%. Student's t test statistics revealed highly significant differences in the values of the peaks and the areas between these two populations ($P<10^{-7}$ for peaks and $P<10^{-8}$ for areas).

Table 1
Number of active voxels, mean signal peak and percentage of nonvenous voxels of each subject (S1–S6) and across all subjects (total)

	S1	S2	S3	S4	S5	S6	Total
Active voxels	48	72	43	154	75	35	427
Mean signal peak (%)	1.2	1.4	1.4	1.5	2.9	2.9	1.8
Nonvenous voxels (%)	56	27	32	39	18	37	35

4. Discussion

The main aim of this work was to better clarify the nature of BOLD functional activation through a highly accurate comparison between activated areas and underlying venous vasculature by means of the methodology described in the Results section. The results found indicate a direct relationship between the BOLD signal intensity and the venous content of active voxels, which is an important feature characterizing the BOLD signal and possibly filtering large vessel artifacts from activation maps. By processing high-resolution datasets and using high-field MRI, it was possible to depict the brain vasculature at a very high resolution, thus giving high sensitivity to the method and obtaining significant and consistent results.

The problem of determining whether BOLD-related activity is of venous nature or corresponds to cortical activation has been addressed using a variety of methodologies [14,18,32]. An experimental approach to the problem requires an accurate depiction of the brain vasculature, in order to properly merge the information of the functional and anatomical datasets.

The analysis of the brain vasculature, however, is made difficult by its complex and intricate architecture [33]: the dimensions of the vessels, in fact, span over four orders of magnitude [34], from several microns of capillaries, to several tens of microns for venules and arterioles, to several hundreds of microns for small pial arteries and veins [35].

Recently, several brain angiography techniques have been described [15]. In our work, the approach used to extract the brain vasculature from the anatomical dataset is based on high-resolution BOLD venographic imaging. Similar attempts have also been reported in literature [36–38]. Differently from techniques based on flow detection such as TOF [39] or PCA [40], BOLD venography uses venous blood as an intrinsic contrast agent — thanks to the paramagnetic properties of dHb.

An early study by Baudendistel et al. [41] at 1.5 T showed the feasibility of comparing BOLD venograms with EPI functional images. In this work, the authors were able to show a close spatial relationship between functionally active areas and the brain vasculature identified through BOLD venography. However, no quantitative analysis of functional signal was provided in this work, nor was the brain vasculature extracted with a segmentation procedure in order to relate it directly with the functional response. Our study expands the possibilities of analysis offered by the joint usage of BOLD venography and EPI functional experiments.

The major feature of BOLD venography is the low MR signal of veins, which makes them easily identifiable in images and well characterized for segmentation purposes.

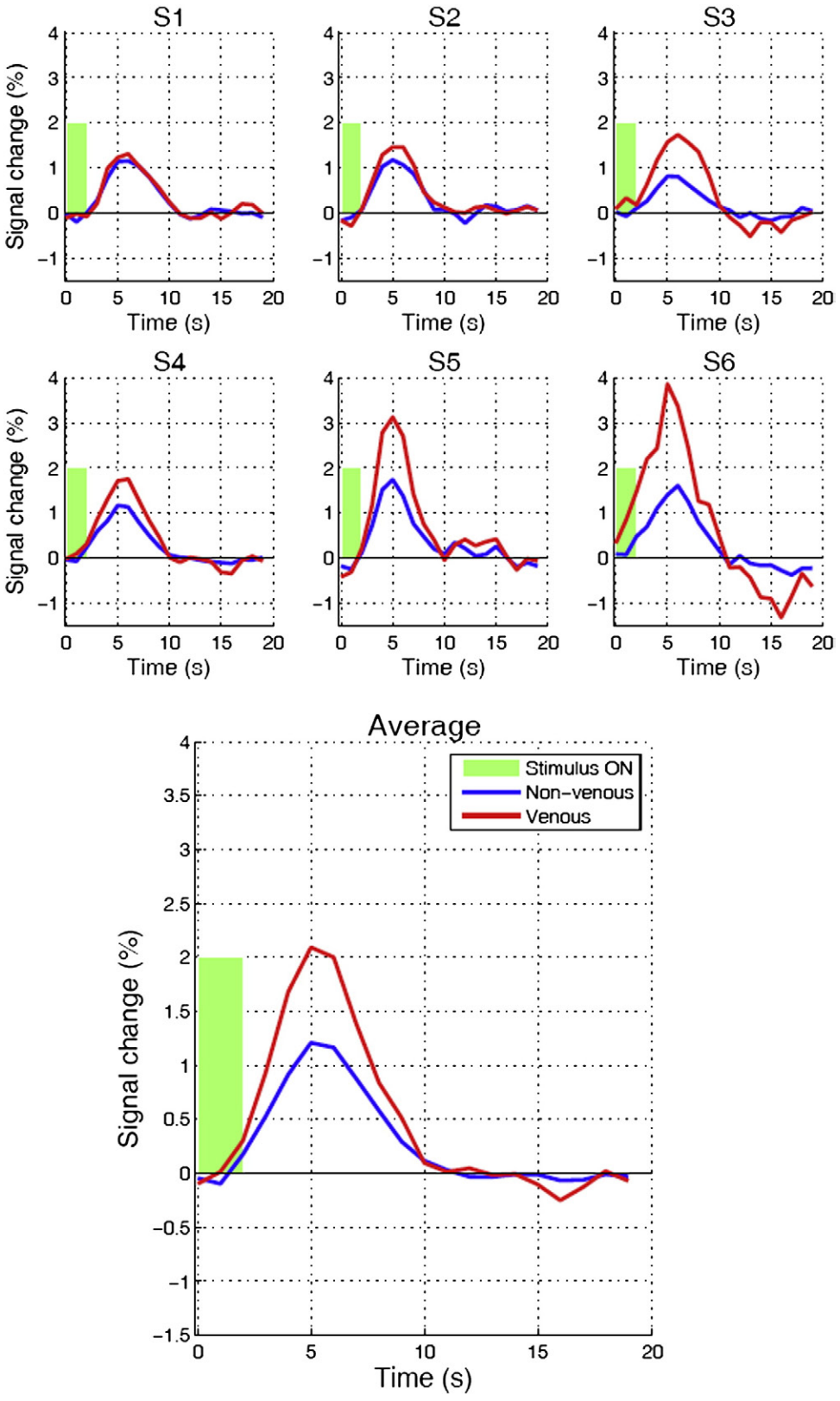

Fig. 2. Plot of the mean time series of all subjects (left; S1–S6) and their average (right). Red and blue curves represent, respectively, venous and nonvenous average time courses, while green areas indicate the period in which the stimulus is on.

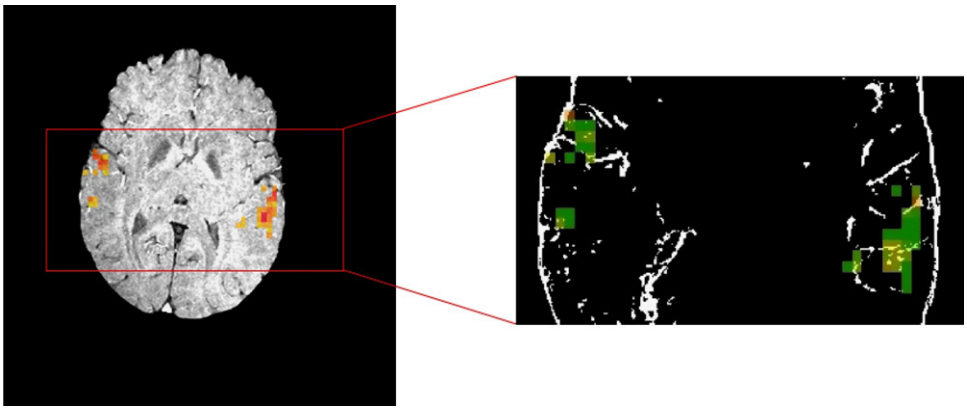

Fig. 3. Activated voxels superimposed on a brain section (left) and the local brain venous vasculature (right). The local vasculature was obtained as a projection of six slices of the brain venogram in order to allow better understanding of the local vascular structures.

Moreover, the use of a high-field magnet at 3 T enhances tissue contrast and the visibility of small vessels [42]. Still, a T_2*-weighted SPGR sequence with short T_R and long T_E, as indicated by Reichenbach and Haacke [38], has a drawback — it gives rise to a low CSF signal, which assumes values comparable with those of venous blood. CSF is, in fact, characterized by long transverse and longitudinal relaxation times [43,44], so that a short T_R tends to suppress CSF signal, while transverse relaxation is negligible on a time scale on the order of tens of milliseconds. Blood relaxation times are shorter than those of CSF [45,46]; in particular, the transverse relaxation rate is quite high such that a rapid blood signal drop is generated. As a result, if a clustering algorithm with three clusters is run on such a dataset, it will segment white matter and gray matter correctly, but it will include venous blood and CSF voxels in the same class.

In order to exclude the CSF from the vein segmentation, we acquired a T_1-weighted dataset to segment the CSF. The good contrast of the T_1-weighted dataset allows for an effective segmentation of CSF by the clustering algorithm. This important information can be obtained with a small increase in the total acquisition time, since the T_1-weighted

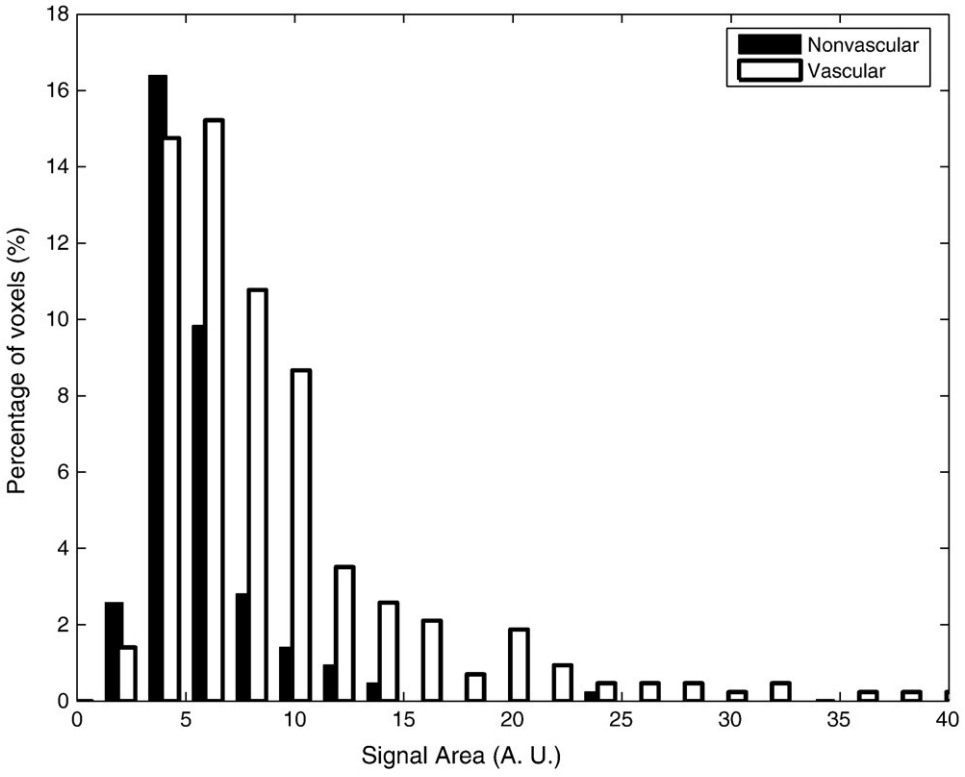

Fig. 4. Histograms of signal peak for vascular and nonvascular voxels across all subjects (n=6).

sequence was very fast (about 3 min) and thus provided limited inconvenience for the subject due to longer acquisition time.

Fuzzy C-means algorithm was chosen for tissue segmentation since it is an easy, effective and unsupervised method [28] that does not need the definition of arbitrary parameters. To improve the results of the segmentation process, the noise content of the anatomical images was reduced through the use of an anisotropic diffusion filter. This filter is able to suppress image noise while at the same time preserving object boundaries [47] — an important feature of the kind of analysis that we performed.

Another issue related to EPI scan is image warping [48]. While warping does not affect the ability to detect functional activation, it can provide imprecise information on the location of cerebral activity. To assess the amount of image distortion, a test was preliminarily performed. On a single subject, EPI images were acquired and then corrected with a procedure similar to that described in Jezzard and Balaban [49]. It was found that in the scanned volume of interest, very little distortion occurred (about 1% in the phase-encoding direction), and the difference in the volume registrations of warped and unwarped images was negligible. It was decided, therefore, not to include in the experimental paradigm a fourth acquisition in order not to lengthen scan time excessively. This decision does not affect, however, the classification of active voxels as "venous" and "nonvenous," since the venogram resolution is much higher than that of functional images, and small misplacing of an active voxel is very unlikely to change its belonging to either class.

The amount of signal drop in a voxel containing venous blood depends on several parameters, such as blood volume fraction and inclination of the vessel with respect to the main magnetic field. It was demonstrated that at 1.5 T (T_R=57 ms, T_E=40 ms, flip angle=25°), the minimum venous volume fraction that makes the voxel signal magnitude significantly lower than that of gray matter is as small as 10–15% [38]. The minimum vessel size that can be detected with the help of BOLD venography can be assessed with a two-compartment model of the BOLD signal. For our experiment, it can be shown that, after phase masking, veins with a blood volume fraction of just 5–10% show significant contrast with brain tissues. With a spatial resolution of 0.5×0.5 mm^2, this means that the methodology is able to detect the presence of a vessel with a diameter around 130–180 μm. The following anisotropic diffusion filtering does not alter the minimum detectable vessel size, since its only effect is to reduce the noise content while preserving image features.

BOLD venography is a powerful technique, but it is still not capable of depicting brain venules in their smallest dimensions. There currently remains great interest in the study of brain microvasculature, as the analysis of the venous structures at the tens-of-microns level has resulted in a useful assessment of angiogenesis [50] and diagnosis of intracranial tumors [51]. For these reasons, other techniques have been

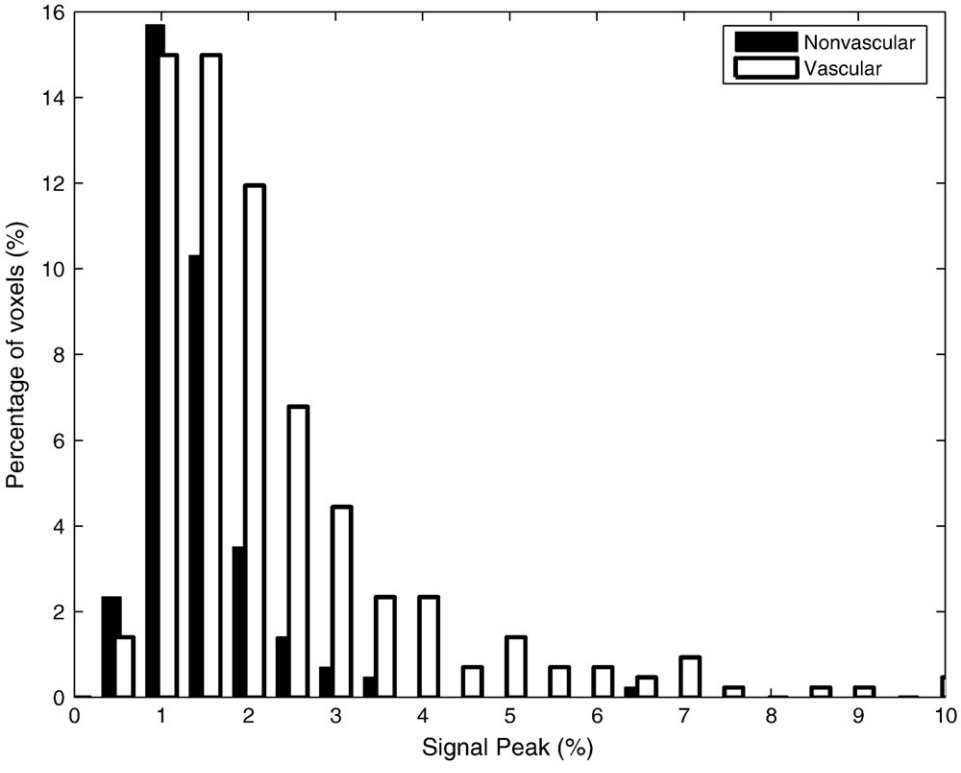

Fig. 5. Histograms of the signal area for vascular and nonvascular voxels across all subjects (n=6).

developed in order to improve the resolution of venograms, utilizing either ultra-high-field scanners [52] or vessel size imaging [53].

Many activated brain areas were found to be concomitant with the brain microvasculature, so that the number of vascular voxels was sufficient to allow for statistical inference. Conversely, it was very helpful to repeat the experimental paradigm a great number of times [20], since the averaging procedure provided signals with a low noise content, permitting a reliable estimation of the signal features (peaks, areas and undershoot) without the need for curve fitting and additional approximation and errors in the assessment.

The maximum signal change in the activated voxels exhibited in each subject a high variability, which, far from being of random nature, was significantly correlated with the variability of the correspondent venous volume fraction. Current theoretical models predict that BOLD functional signal is bound to increase with increasing blood volume fraction [54]. A higher voxel venous content enhances, in fact, the intravascular contribution to BOLD signal and, at the same time, broadens the volume in which the extravascular effect is active. However, if the vessel is large enough, part of the volume affected by the extravascular effect might extend beyond the voxel limits and have no influence on the voxel signal. If the blood volume fraction is further increased, the increase in the intravascular contribution is counterbalanced by the reduction in the extravascular contribution, and the BOLD signal shows no net increase. In this situation, the long-range effect of large vessels is such that a BOLD signal is measured in the neighboring pixels; this is consistent with the fact that BOLD signal enhancement has been observed in areas with no vessels but close to vascular structures [55].

Although the relationship between BOLD functional response and blood volume fraction is straightforward, in practice, several other phenomena influence the measured BOLD signal, including diffusion [56], inflow effects [57], blood pulsatility [58], scanner noise [59] and so on. As a result, the measured signal may differ from what it is expected, since each of these sources of noise has a different impact on BOLD signal according to the vessel size.

The capability of BOLD fMRI to detect specifically cerebral active areas is related to the extent of the region in which hemodynamic changes occur. Functional activation following external stimulation induces local modifications in blood flow and oxygenation of the capillary beds adjacent to neuronal activity, but these changes may propagate downstream in the brain vasculature and appear in large draining vessels far from the original active areas [60,61]. To increase the specificity of BOLD functional analysis, it is necessary to eliminate, therefore, the macrovascular contribution.

The intravascular and extravascular contributions to BOLD functional signal appear in both small and large vessels [32,62,63]. GE and spin-echo (SE) functional techniques, though, are differently sensitive to these contributions, since SE techniques refocus static spin dephasing around the vessels, thus eliminating selectively the extravascular signal coming from large vessels . The intravascular contribution is present instead with both techniques, since it is due to the increase in blood T_2 and T_2* caused by oxygenation increase.

The intravascular contribution can be eliminated by using high-magnetic-field imaging, since blood transversal relaxation rate increases much faster than that of other tissues with increasing field strength [64]. The intravascular contribution to the BOLD functional signal can be assessed through diffusion-weighted functional experiments: with this approach, it was demonstrated that, at low-field blood, effects on large vessels are the largest sources of BOLD signal [65,66]. The results of our work are therefore coherent with these findings. At higher fields, it is possible to completely suppress blood signal with a correct choice of echo time [67,68].

In three of the six subjects, a poststimulus undershoot was observed in the mean signal. This phenomenon, observed already in the earliest studies on fMRI [2,69], is explained through delayed postactivation vascular compliance [70,71] caused by transient uncoupling of oxygen metabolism and blood flow [72]. Noticeably, although the model function used to detect functional activation ignores the presence of a poststimulus undershoot, it was able to detect activated areas correctly.

The experimental correlation found between venous blood and BOLD response intensity stresses the role of venous blood as a major source of functional BOLD signal. Venous artifacts filtering based on BOLD response intensity thus finds a further experimental fundament in the results of this work. In agreement with the results of Hlustik et al. [14], in fact, it was evidenced how the response intensity of parenchymal activation tends to show a different range of values compared to vascular activation, and that vessels with different sizes give rise to different signals. However, as observed also by Hall et al. [18], venous BOLD signal is more intense only on a statistical basis, so that effective separation of venous-activated voxels is not immediate. To this purpose, other features of the BOLD signal, such as signal phase [73,74] or signal delay [75], have also been investigated.

Signal delay, in particular, has been considered indicative of BOLD signal nature, since, in large draining vessels, the hemodynamic changes that originate BOLD contrast occur on a longer time scale [24]. It is still under debate as to whether this property can be effectively used to discriminate venous vessels in BOLD maps, although an early study [75] seemed to demonstrate that this could be a viable option. However, successive studies found that the distributions of delay and response intensity across different tissues are not very different [18] and that longer venous delays occur on average and not for each single voxel [76,77], resulting in overlap in delays for venous and nonvenous regions.

Our study focused on investigating the relationship between functional response intensity and brain vasculature, so the experimental paradigm was designed to characterize in the best way the response signal intensity, and not other features of the functional signal such as signal delay. However, it was found that, in all subjects, venous voxels have a larger average delay, although the delay difference results within the sampling time. It must be considered anyway that, in our work, the functional response was characterized with parameters measured directly on the original time series, so that all timings are necessarily expressed as multiples of the repetition time T_R. Besides, an inspection of time courses shows that their noise content is too high to calculate the time-to-peak directly, since the time series evidence signal deviations from a theoretical "smooth" curve. Noise suppression through time series averaging was therefore effective as far as response intensity was concerned, while it was not as effective when assessing the signal time-to-peak. To correctly estimate this parameter, other data processing procedures such as frequency filtering or curve fitting would be required. This is, however, beyond the scope of our work.

In conclusion, this methodology exploits advanced high-resolution venographic techniques to provide characterization of the BOLD signal, which is useful in discriminating large draining vessels and in suppressing venous artifacts in activation maps. In this way, more precise and reliable information on the location and extent of activated areas can be obtained from fMRI studies. The method described in this article could be included among the techniques of neuro-functional image processing, as the principles on which this method is established are general and have no reference to a specific kind of functional experiment.

Acknowledgments

We wish to thank Dr. Tommaso Scarabino, Dr. Teresa Popolizio and all people working at the neuroradiologic center of Instituto di Recovero e Cura a Carattere Scientifico (IRCCS) Casa Sollievo della Sofferenza of San Giovanni Rotondo (Foggia, Italy) for their kind collaboration. We are deeply grateful to all our healthy volunteers who agreed to be subjects of this study for the advancement of science.

This work was partially funded by the Fondo per gli Investimenti della Ricerca di Base grant no. RBNE01E9ZR; CERSUM Laboratory Rif. Min. Decreto Direttoriale 1105/2002 no. 243; and Noninvasive Medical Imaging, Innovative Technologies and Advanced Medical Diagnostics Laboratory Rif. Min. DD MIUR 14.5.2005 no. 602–DM18640 from the Italian Ministry of Research.

References

[1] Ogawa S, Lee TM, Kay AR, Tank DW. Brain magnetic resonance imaging with contrast dependent on blood oxygenation. Proc Natl Acad Sci U S A 1990;87:9868–72.

[2] Kwong KK, Belliveau JW, Chesler DA, Goldberg IE, Weisskoff RM, Poncelet BP, et al. Dynamic magnetic resonance imaging of human brain activity during primary sensory stimulation. Proc Natl Acad Sci U S A 1992;89:5675–9.

[3] Hammeke TA. Functional MRI in neurology. In: Moonen CTW, Bandettini PA, editors. Functional MRI. Berlin: Springer Verlag; 1999. p. 4754–86.

[4] Lee SP, Silva AC, Ugurbil K, Kim SG. Diffusion-weighted spin-echo fMRI at 9.4 T: microvascular/tissue contribution to BOLD signal changes. Magn Reson Med 1999;42:919–28.

[5] Logothetis NK, Pauls J, Augath M, Trinath T, Oeltermann A. Neurophysiological investigation of the basis of the fMRI signal. Nature 2001;412:150–7.

[6] Ogawa S, Menon RS, Tank DW, Kim SG, Merkle H, Ellermann JM, et al. Functional brain mapping by blood oxygenation level-dependent contrast magnetic resonance imaging. A comparison of signal characteristics with a biophysical model. Biophys J 1993;64:803–12.

[7] Bauer WR, Nadler W, Bock M, Schad LR, Wacker C, Hartlep A, et al. The relationship between the BOLD-induced $T(2)$ and $T(2)(*)$: a theoretical approach for the vasculature of myocardium. Magn Reson Med 1999;42:1004–10.

[8] Davis TL, Kwong KK, Weisskoff RM, Rosen BR. Calibrated functional MRI: mapping the dynamics of oxidative metabolism. Proc Nat Acad Sci U S A 1998;95:1834–9.

[9] Kim SG, Rostrup E, Larsson HBW, Ogawa S, Paulson PB. Determination of relative $CMRO_2$ from CBF and BOLD changes: significant increase of oxygen consumption rate during visual stimulation. Magn Reson Med 1999;41:1152–61.

[10] Matthews PM. An introduction to functional magnetic resonance imaging of the brain. In: Jezzard P, Matthews PM, Smith SM, editors. Functional MRI — an introduction to methods. Oxford: Oxford University Press; 2002. p. 3–34.

[11] Malonek D, Grinvald A. Interactions between electrical activity and cortical microcirculation revealed by imaging spectroscopy: implications for functional brain mapping. Science 1996;272:551–4.

[12] Frahm J, Merboldt KD, Hanicke W, Kleinschmidt A, Boecker H. Brain or vein — oxygenation or flow? On signal physiology in functional MRI of human brain activation. NMR Biomed 1994;7:45–53.

[13] Vlieger EJ, Majoie CB, Leenstra S, Den Heeten GJ. Functional magnetic resonance imaging for neurosurgical planning in neurooncology. Eur Radiol 2004;14:1143–53.

[14] Hlustik P, Noll DC, Small SL. Suppression of vascular artifacts in functional magnetic resonance images using MR angiograms. Neuroimage 1997;7:224–31.

[15] Pui MH. Cerebral MR venography. Clin Imaging 2004;28:85–9.

[16] Graves MJ. Magnetic resonance angiography. Br J Radiol 1997;70:6–28.

[17] Krings T, Erberich S, Roessler F, Reul J, Thron A. MR blood oxygenation level-dependent signal differences in parenchymal and large draining vessels: implications for functional MR imaging. Am J Neuroradiol 1999;20:1907–14.

[18] Hall DA, Gonçalves MS, Smith S, Jezzard P, Haggard MP, Kornak J. A method for determining venous contribution to BOLD contrast sensory activation. Magn Reson Imaging 2002;20:695–706.

[19] Reichenbach JR, Venkatesan R, Yablonskiy DA, Thompson MR, Lai S, Haacke EM. Theory and application of static field inhomogeneity effects in gradient-echo imaging. J Magn Reson Imaging 1997;7:266–79.

[20] Mechelli A, Henson RN, Price CJ, Friston KJ. Comparing event-related and epoch analysis in blocked design fMRI. Neuroimage 2003;18:806–10.

[21] Bilecen D, Seifritz E, Scheffler K, Henning J, Schulte AC. Amplitopicity of the human auditory cortex: an fMRI study. Neuroimage 2002;17:710–8.

[22] Bandettini PA, Jesmanowicz A, Wong EC, Hyde JS. Processing strategies for time-course data sets in functional MRI of the human brain. Magn Reson Med 1993;30:161–73.

[23] Cohen MS. Parametric analysis of fMRI data using linear systems methods. Neuroimage 1997;6:93–103.
[24] Bandettini PA, Cox RW. Event-related fMRI contrast when using constant interstimulus interval: theory and experiment. Magn Res Med 2000;43:540–8.
[25] Cohen MS. Echo-planar imaging and functional MRI. In: Moonen CTW, Bandettini PA, editors. Functional MRI. Berlin: Springer Verlag; 2002. p. 137–48.
[26] Cox R. AFNI: software for analysis and visualization of functional magnetic resonance neuroimages. Comput Biomed Res 1996;29: 162–73.
[27] Gerig G, Kubler O, Jolesz FA. Nonlinear anisotropic filtering of MRI data. IEEE Trans Med Imaging 1992;11:221–32.
[28] Bezdek J, Hall L, Clarke L. Review of MR image segmentation using pattern recognition. Med Phys 1993;20:1033–48.
[29] Phillips WE, Velthuizen RP, Phuphanich S, Hall LO, Clarke LP, Silbiger ML. Application of fuzzy C-means segmentation technique for tissue differentiation in MR images of a hemorrhagic glioblastoma multiforme. Magn Reson Imaging 1995;13:277–90.
[30] Ogawa S, Lee TM, Nayak AS, Glynn P. Oxygenation-sensitive contrast in magnetic resonance image of rodent brain at high magnetic fields. Magn Reson Med 1990;14:68–78.
[31] Robson MD, Dorosz JL, Gore JC. Measurement of the temporal fMRI response of the human auditory cortex to trains of tones. Neuroimage 1998;7:185–98.
[32] Oja JME, Gillen J, Kauppinen RA, Kraut M, van Zijl PCM. Venous blood effects in spin-echo fMRI of human brain. Magn Res Med 1999; 42:617–26.
[33] Salamon G, Huang YP. Radiological anatomy of the brain. Berlin: Springer Verlag; 1976.
[34] Buxton RB. Introduction to functional magnetic resonance imaging — principles and techniques. Cambridge: Cambridge University Press; 2002.
[35] Berne RM, Levi MN. The circuitry. In: Berne RM, Levi MN, editors. Physiology. St. Louis: Mosby; 1988. p. 395–7.
[36] Cho ZH, Ro YM, Lim TH. NMR venography using the susceptibility effect produced by deoxyhemoglobin. Magn Reson Med 1992;28: 25–38.
[37] Essig M, Reichenbach JR, Schad LR, Schoenberg SO, Debus J, Kaiser WA. High-resolution MR venography of cerebral arteriovenous malformations. Magn Reson Imaging 1999;17:1417–25.
[38] Reichenbach JR, Haacke EM. High-resolution BOLD venographic imaging: a window into brain function. NMR Biomed 2001;14: 453–67.
[39] Lewin JS, Masaryk TJ, Smith AS, Ruggieri PM, Ross JS. Time-of-flight intracranial MR venography: evaluation of the sequential oblique section technique. Am J Neuroradiol 1994;15:1657–64.
[40] Liauw L, Van Buchem MA, Spilt A, De Bruine FT, Van den Berg R, Hermans J, et al. MR angiography of the intracranial venous system. Radiology 2000;214:678–82.
[41] Baudendistel KT, Reichenbach JR, Metzner R, Schroeder J, Schad LR. Comparison of functional MR-venography and EPI-BOLD fMRI at 1.5 T. Magn Reson Imaging 1998;16(8):989–91.
[42] Reichenbach JR, Barth M, Haacke EM, Klarhofer M, Kaiser WA, Moser E. High-resolution MR venography at 3.0 Tesla. J Comput Assist Tomogr 2000;24:949–57.
[43] Luh WM, Wong EC, Bandettini PA, Ward D, Hyde JS. Comparison of simultaneously measured perfusion and BOLD signal increases during brain activation with T_1-based tissue identification. Magn Reson Med 2000;44:137–43.
[44] Zhao X, Bodurka J, Jesmanowicz A, Li SJ. B_0-fluctuation-induced temporal variation in EPI image series due to the disturbance of steady-state free precession. Magn Reson Med 2000; 44:758–65.
[45] Stanisz GJ, Odrobina EE, Pun J, Escaravage M, Graham SJ, Bronskill MJ, et al. T_1, T_2 relaxation and magnetization transfer in tissue at 3 T. Magn Reson Med 2005;54:507–12.
[46] Schwarzbauer C, Heinke W. Investigating the dependence of BOLD contrast on oxidative metabolism. Magn Reson Med 1999;41:537–43.
[47] Zingale R, Zingale A. Detection of MRI brain contour using isotropic and anisotropic diffusion filter. A comparative study. J Neurosurg Sci 1998;42:111–4.
[48] Hutton C, Bork A, Josephs O, Deichmann R, Ashburner J, Turner R. Image distortion correction in fMRI: a quantitative evaluation. Neuroimage 2002;16(1):217–40.
[49] Jezzard P, Balaban RS. Correction for geometric distortion in echo planar images from B_0 field variations. Magn Reson Med 1995;34(1): 65–73.
[50] Kleihues P, Burger PC, Plate KH, Ohgaki H, Cavanee WK. Glioblastoma. In: Kleihues P, Cavenee WK, editors. Pathology and genetics of tumours of the nervous system. Lyon: International Agency for Research on Cancer; 1997.
[51] Sugahara T, Korogi Y, Kochi M, Ushio Y, Takahashi M. Perfusion-sensitive MR imaging of gliomas: comparison between gradient-echo and spin-echo echo-planar imaging techniques. Am J Neuroradiol 2001;22:1306–15.
[52] Christoforidis GA, Kangarlu A, Abduljalil AM, Schmalbrock P, Chaudhry A, Yates A, et al. Susceptibility-base imaging of glioblastoma microvascularity at 8 T: correlation of MR imaging and postmortem pathology. Am J Neuroradiol 2004;25:756–60.
[53] Kiselev VG, Strecker R, Ziyeh S, Speck O, Hennig J. Vessel size imaging. Magn Reson Med 2005;53:553–63.
[54] Lai S, Glover GH, Haacke EM. Spatial selectivity of BOLD contrast: effects in and around the vessels. In: Moonen CTW, Bandettini PA, editors. Functional MRI. Berlin: Springer Verlag; 2000. p. 221–32.
[55] Haacke EM, Hopkins A, Lai S, Buckley P, Friedman L, Meltzer H, et al. 2D and 3D high resolution gradient echo functional imaging of the brain: venous contributions to signal in motor cortex studies. NMR Biomed 1994;7:54–62.
[56] Fujita N. Extravascular contribution of blood oxygenation level-dependent signal changes: a numerical analysis based on a vascular network model. Magn Reson Med 2001;46:723–34.
[57] Duyn JH, Moonen CTW, van Yperen GH, de Boer RW, Luyten PR. Inflow versus deoxyhemoglobin effects in BOLD functional MRI using gradient echoes at 1.5 T. NMR Biomed 1994;7:83–8.
[58] Dagli MS, Ingleholm JE, Haxby JV. Localization of cardiac-induced signal change in fMRI. Neuroimage 1999;9:407–15.
[59] Wolak T, Bogorodzki P, Piatkowska-Janko EM, Orzechowski M, Kurjata R, Golebiowski M, et al. Analysis of the BOLD responses from human primary auditory cortex using cytoarchitectonic maximum probability maps. Book of abstracts: ESMRMB 22nd Annual Scientific Meeting, Basle. Magnetic Resonance Materials in Physics, Biology and Medicine, Vol. 18, Suppl 1. Berlin/Heidelberg: Springer; 2005.
[60] Duong TQ, Kim DS, Ugurbil K, Kim SG. Spatio-temporal dynamics of the BOLD fMRI signals in cat visual cortex: toward mapping columnar structures using the early negative response. Magn Reson Med 2000; 44:231–42.
[61] Duong TQ, Kim DS, Ugurbil K, Kim SG. Localized blood flow response at sub-millimeter columnar resolution. Proc Natl Acad Sci USA 2001;98:10904–9.
[62] Ugurbil K, Hu X, Chen W, Zhu XH, Kim SG, Georgopoulos A. Functional mapping in the human brain using high magnetic fields. Philos Trans R Soc Lond B 1999;354:1195–213.
[63] Ogawa S, Menon RS, Kim SG, Ugurbil K. On the characteristics of functional magnetic resonance imaging of the brain. Annu Rev Biophys Biomol Struct 1998;27:447–74.
[64] Thulborn KR, Waterton JC, Mattews PM, Radda GK. Oxygenation dependence of the transverse relaxation time of water protons in whole blood at high field. Biochem Biophys Acta 1982;714:265–70.
[65] Song AW, Wong EC, Tan SG, Hyde JS. Diffusion-weighted fMRI at 1.5 T. Magn Reson Med 1996;35:155–8.
[66] Boxerman JL, Bandettini PA, Kwong KK, Baker JR, Davis TL, Rosen BR, et al. The intravascular contribution to fMRI signal change: Monte

Carlo modeling and diffusion-weighted studies in vivo. Magn Reson Med 1995;34:4–10.
[67] Duong TQ, Yacoub E, Adriany G, Hu X, Ugurbil K, Kim SG. Microvascular BOLD contribution at 4 and 7 T in the human brain: gradient-echo and spin-echo fMRI with suppression of blood effects. Magn Reson Med 2003;49(6):1019–27.
[68] Lee SP, Silva AC, Ugurbil K, Kim SG. Diffusion-weighted spin-echo fMRI at 9.4 T: microvascular/tissue contribution to BOLD signal change. Magn Reson Med 1999;42:919–28.
[69] Ogawa S, Tank DW, Menon R, Ellermann JM, Kim SG, Merkle H, et al. Intrinsic signal changes accompanying sensory stimulation: functional brain mapping with magnetic resonance imaging. Proc Natl Acad Sci U S A 1992;89:5951–5.
[70] Buxton RB, Wong EC, Frank LR. Dynamics of blood flow and oxygenation changes during brain activation: the balloon model. Magn Reson Med 1998;39:855–64.
[71] Mandeville JB, Marota JJ, Ayata C, Zaharchuk G, Moskowitz MA, Rosen BR, et al. Evidence of a cerebrovascular postarteriole windkessel with delayed compliance. J Cereb Blood Flow Metab 1999;19:679–89.
[72] Frahm J, Kruger G, Merboldt KD, Kleinschmidt A. Dynamic uncoupling and recoupling of perfusion and oxidative metabolism during focal brain activation in man. Magn Reson Med 1996;35:143–8.
[73] Lai S, Reichenbach JR, Haacke EM. Commutator filter: a novel technique for the identification of structures producing significant susceptibility inhomogeneities and its application to functional MRI. Magn Reson Med 1996;36:781–7.
[74] Menon RS. Postacquisition suppression of large-vessel BOLD signals in high-resolution fMRI. Magn Reson Med 2002;47:1–9.
[75] Lee AT, Glover GH. Discrimination of large venous vessels in time-course spiral blood oxygen dependent magnetic resonance neuroimaging. Magn Reson Med 1995;33:745–54.
[76] Kruggel F, von Cramon DY. Temporal properties of the hemodynamic response in functional MRI. Hum Br Map 1999;8:259–71.
[77] Saad ZS, Ropella KM, Cox RW, De Yoe EA. Analysis and use of fMRI response delays. Hum Brain Mapp 2001;13:74–93.